FORMULATION, OPTIMIZATION, AND EVALUATION OF A POLYHERBAL EMULGEL CONTAINING METHANOLIC STEM-BARK EXTRACTS OF *LIMONIA ACIDISSIMA*, *MORINGA OLEIFERA*, AND *PITHECELLOBIUM DULCE*

Shankar Khandare[1]*, Ramakant Sharma[1], Sudha Vengurlekar[1], Sachin Kumar Jain[1]
[1]Department of Pharmacy, Oriental University, Indore, Madhya Pradesh, India

*** Corresponding Author**
Shankar Khandare
Department of Pharmacy, Oriental University, Indore, M.P. India
Email: sskhandare77@gmail.com

Abstract
The present study aimed to formulate, statistically optimize, and evaluate a polyherbal emulgel containing methanolic stem bark extracts of *Limonia acidissima*, *Moringa oleifera*, and *Pithecellobium dulce* for topical drug delivery. Preformulation studies identified sesame oil as the most suitable oil phase owing to its highest apparent solubility (>40 mg/mL), while Tween 80 and propylene glycol exhibited superior emulsification efficiency, with transmittance values of 72.55% and 51.46%, respectively. A three-level factorial design coupled with response surface methodology was employed to optimize the formulation by investigating the effects of oil concentration and surfactant/co-surfactant mixture (Smix) on particle size, zeta potential, and entrapment efficiency. Numerical optimization predicted an optimized formulation containing 2.62 mL of oil and 4.11 mL of Smix with an overall desirability of 1.000. Experimental validation demonstrated good agreement between the predicted and observed responses, yielding a particle size of 78.06 nm, zeta potential of −32.24 mV, and entrapment efficiency of 87.40%. The optimized nanoemulsion was successfully incorporated into a Carbopol® 940 gel base to prepare polyherbal emulgel formulations (F1–F4). The developed emulgels exhibited a creamish appearance, excellent homogeneity, skin-compatible pH (6.15–6.30), viscosity ranging from 33,200 to 37,800 cP, and spreadability between 4.7 and 5.8 g·cm/s, indicating suitable physicochemical characteristics for topical application. Overall, the study demonstrates that the Quality-by-Design approach effectively optimized the formulation variables and produced a stable polyherbal emulgel with desirable physicochemical properties, providing a promising platform for subsequent pharmacological evaluation in wound healing and antimicrobial applications.

Keywords: *polyherbal emulgel; factorial design; sesame oil; Tween 80; propylene glycol.*

How to cite this article: Khandare S, Sharma R, Vengurlekar S, Jain SK. Formulation, optimization, and evaluation of a polyherbal emulgel containing methanolic stem-bark extracts of Limonia acidissima, Moringa oleifera, and Pithecellobium dulce. Int J Drug Deliv Technol. 2026;16(72s): 225-239. DOI: 10.25258/ijddt.16.72s.27

1. Introduction

Topical drug delivery offers several advantages over systemic therapy by delivering high concentrations of therapeutic agents directly to the wound site while minimizing systemic exposure and associated adverse effects. Conventional topical dosage forms, including creams, ointments, and gels, are widely used for wound management; however, they often exhibit limitations such as poor penetration of active constituents, inadequate residence time, limited physical stability, and reduced bioavailability, particularly for lipophilic phytoconstituents. These shortcomings have stimulated the development of advanced nanocarrier-based drug delivery systems that improve solubilization, enhance skin permeation, and provide sustained local drug release, thereby increasing therapeutic efficacy in wound management [1]. Nanoemulsions have gained considerable attention as effective topical drug delivery systems because of their nanosized droplets, large interfacial surface area, high kinetic stability, and excellent ability to solubilize poorly water-soluble bioactive compounds. Their small droplet size facilitates enhanced dermal penetration and improves the bioavailability of encapsulated phytoconstituents. However, the inherently low viscosity of nanoemulsions limits their retention at the site of application. Incorporation of nanoemulsions into a hydrogel matrix results in an emulgel, a hybrid delivery system that combines the superior penetration characteristics of nanoemulsions with the favorable rheological properties of gels. This approach enhances spreadability, prolongs residence time, improves patient compliance, and enables sustained release of therapeutic agents, making emulgels particularly suitable for topical wound-healing applications [2]. Medicinal plants have long been recognized as valuable sources of bioactive compounds with antioxidant, antimicrobial, anti-inflammatory, and tissue regenerative properties. Polyherbal formulations have attracted increasing scientific interest because they combine multiple medicinal plants to produce synergistic therapeutic

effects through complementary mechanisms of action. Such formulations can simultaneously modulate oxidative stress, suppress microbial proliferation, reduce inflammation, stimulate collagen synthesis, promote angiogenesis, and accelerate re-epithelialization, thereby improving the overall wound-healing process. Consequently, polyherbal topical formulations represent a promising alternative to conventional wound management strategies [3]. The stem bark extracts of *Limonia acidissima, Moringa oleifera*, and *Pithecellobium dulce* are rich sources of flavonoids, phenolic compounds, tannins, alkaloids, and other secondary metabolites that have been reported to possess potent antioxidant, antimicrobial, anti-inflammatory, and wound-healing activities. The combination of these medicinal plants in a single formulation is expected to provide synergistic pharmacological effects, resulting in enhanced therapeutic efficacy while overcoming the limitations associated with individual herbal extracts. Such a polyherbal approach may therefore offer a more effective strategy for promoting wound repair and preventing microbial infection [4]. The successful development of nanoemulsion-based topical formulations depends on the appropriate selection and optimization of critical formulation variables, including the oil phase, surfactant, co-surfactant, and their relative proportions. These formulation components significantly influence critical quality attributes such as particle size, zeta potential, entrapment efficiency, physical stability, and drug release behavior. Modern pharmaceutical formulation development therefore follows the Quality-by-Design (QbD) paradigm, in which Design of Experiments (DoE) and Response Surface Methodology (RSM) are employed to establish mathematical relationships between formulation variables and product quality attributes. These statistical approaches improve formulation robustness, reproducibility, and optimization efficiency while minimizing experimental variability and development time [5]. Based on these considerations, the present study aimed to formulate, statistically optimize, and evaluate a polyherbal emulgel containing methanolic stem bark extracts of *Limonia acidissima*, *Moringa oleifera*, and *Pithecellobium dulce*. Preformulation studies were performed to identify the most suitable oil phase, surfactant, and co-surfactant, followed by optimization using a three-level factorial Design of Experiments. The optimized nanoemulsion was subsequently incorporated into a Carbopol® 940 gel matrix to develop a polyherbal emulgel, which was evaluated for its physicochemical characteristics, including particle size, zeta potential, entrapment efficiency, pH, viscosity, spreadability, and homogeneity, to establish its suitability as a promising topical drug delivery system for wound management [6].

2. Materials and Methods

2.1. Preformulation Investigation.

Solubility Study.

The apparent solubility of the polyherbal extract comprising *Pithecellobium dulce*, *Limonia acidissima*, and *Moringa oleifera* stem bark was determined in various oil systems using the shake-flask method. Briefly, an excess amount of the polyherbal extract was added to 2 mL of each selected oil in sealed glass vials and mixed using a vortex mixer. The mixtures were equilibrated in a thermostatically controlled shaking water bath at 25 ± 1°C for 48 h to attain equilibrium. Following equilibration, the samples were centrifuged at 5000 rpm for 10 min, and the supernatants were filtered through a 0.22 μm syringe filter (Whatman, UK). The concentration of dissolved extract was determined spectrophotometrically, and the oil exhibiting the highest solubility was selected for subsequent nanoemulsion formulation [7].

Emulsification Efficiency

The emulsification efficiency of different surfactants and co-surfactants was evaluated by determining their ability to emulsify the selected oil phase. Briefly, 10 μL of the selected oil was gradually added to 5% (w/v) aqueous solutions of individual surfactants or co-surfactants under continuous vortex mixing until persistent turbidity was observed. The prepared oil-in-water emulsions were allowed to equilibrate, and their percentage transmittance (%T) was measured at 650 nm using a UV–Visible spectrophotometer. The surfactant and co-surfactant exhibiting the highest transmittance values and producing stable, homogeneous emulsions without phase separation were selected for further formulation studies [8].

2.2. Preparation of *Pithecellobium dulce*, *Limonia acidissima*, and *Moringa oleifera* Loaded Polyherbal Nanoemulsion.

The polyherbal nanoemulsion was prepared by the probe sonication method. The required quantities of *Pithecellobium dulce*, *Limonia acidissima*, and *Moringa oleifera* stem bark extracts were initially dissolved in a small volume of ethanol to obtain a clear solution. This solution was incorporated into the selected oil phase under continuous magnetic stirring. Separately, the aqueous phase was prepared by dissolving Tween 80 and propylene glycol in distilled water. Both phases were heated separately to 60–65°C and subsequently mixed by slowly adding the oil phase to the aqueous phase under magnetic stirring at 1000 rpm for 20 min to obtain a coarse emulsion. The coarse emulsion was further homogenized at 5000 rpm for 10 min, followed by probe sonication at 20 kHz with 40–60% amplitude for 5 min in pulse mode (10 s ON/5 s OFF) while maintaining the formulation in an ice bath to prevent thermal degradation of the phytoconstituents. The resulting nanoemulsion was allowed to cool to room temperature and stored in airtight containers until further physicochemical evaluation [9].

Table 1. Trial formulations used during preliminary nanoemulsions development.

Trial No.	Drug (mg)	Sesame Oil (mL)	Tween 80 (mL)	Propylene Glycol (mL)	Smix Ratio	Water q.s. to	Sonication (min)
PH-NE 1	45	1.0	2.0	1.0	2:1	10 mL	5
PH-NE 2	45	1.5	2.5	1.25	2:1	10 mL	5
PH-NE 3	45	2.0	3.0	1.5	2:1	10 mL	5
PH-NE 4	45	2.5	3.5	1.75	2:1	10 mL	5
PH-NE 5	45	3.0	4.0	2.0	2:1	10 mL	5
PH-NE 6	45	3.5	4.5	2.25	2:1	10 mL	5
PH-NE 7	45	2.0	2.0	1.0	2:1	10 mL	5
PH-NE 8	45	2.0	2.5	1.25	2:1	10 mL	5
PH-NE 9	45	2.0	3.0	1.5	2:1	10 mL	5
PH-NE 10	45	2.0	3.5	1.75	2:1	10 mL	5

2.3. Experimental design and optimization

PHE-loaded nanoemulsion formulations were developed using the high energy method by the 3-level factorial design. The independent factors in the study included concentration of oil and surfactant and cosurfactant ratio (s mix), each with three levels (high, medium and low). Particle size (PS), Zeta potential (ZP) and entrapment efficiency (EE) were the dependent variables. The 3-level factorial design and variables were selected based on literature reviews and prior trial experiments. To obtain optimized formulation of PHE-loaded nanoemulsion the effects of the independent factors on the response variables were assessed using the statistical package Design-Expert® version 25.0.0 64-bit software (Stat Ease Inc., Minneapolis, MN).

Table 2. Independent variables and factor levels used for optimization.

Factors	Independent Variables	Low (-1)	Middle (0)	High (+1)
X_1	Oil (mL)	1	3	5
X_2	Smix (mL)	4	5	6

Table 3. Dependent variables and optimization constraints

Response	Dependent variable	Constraint
Y1	Particle size (nm)	Minimum
Y2	Zeta potential (mV)	Maximum magnitude
Y3	Entrapment efficiency (%)	Maximum

2.4. Optimization (formula selection) of Nanoemulsion

Numerical optimization was performed using the point prediction function of Design-Expert® software to identify the optimum combination of independent variables capable of producing the minimum particle size, maximum zeta potential (absolute value), and maximum entrapment efficiency. The optimization criteria were established by assigning particle size to be minimized, while the magnitude of zeta potential and entrapment efficiency were set to be maximized. Desirability and contour plots generated by the software were used to identify the optimal design space and predict the optimized formulation. Based on the responses obtained from all 13 experimental runs and the predefined optimization constraints, the formulation exhibiting the highest overall desirability was selected as the optimized nanoemulsion. The optimized formulation was subsequently prepared under the predicted conditions and evaluated for particle size, polydispersity index (PDI), zeta potential, and entrapment efficiency. The experimentally observed responses were compared with the software-predicted values to validate the optimization model and assess the predictive accuracy of the Design of Experiments (DoE) approach [10].

Table 4. Optimized formulation suggested by DOE

Material	A: Oil	B: S mix
Formula	2.62	4.11

2.5. Preparation of Optimized Polyherbal Nanoemulsion.

The optimized polyherbal nanoemulsion was prepared according to the composition predicted by the Design of Experiments (DoE) optimization study. The required quantity of the polyherbal extract was accurately weighed and dissolved in the optimized quantity of sesame oil. The surfactant (Tween 80) and co-surfactant (propylene glycol) were mixed in the optimized ratio to prepare the surfactant mixture (Smix). The oil phase containing the dissolved polyherbal extract was gradually mixed with the Smix under continuous magnetic stirring until a clear and homogeneous mixture was obtained. Purified water was then added dropwise to the oil–Smix mixture under continuous stirring (800–1000 rpm) at room temperature to form a coarse emulsion. The coarse emulsion was further homogenized using a high-speed homogenizer at 5000 rpm for 10 min and subsequently subjected to probe sonication (20 kHz, 40–60% amplitude) for 5 min in pulse mode (10 s ON/5 s OFF) while maintaining the formulation in an ice bath to obtain a stable nanoemulsion. The optimized nanoemulsion was stored in airtight containers at room temperature until further evaluation. Based on the optimized composition, four nanoemulsion formulations containing 0.5%, 1%, 3%, and 5% (w/v) polyherbal extract were prepared by proportionally varying the extract concentration while maintaining constant quantities of the oil phase, Smix, and aqueous phase. The prepared formulations were evaluated for particle size, polydispersity index (PDI), zeta potential, and entrapment efficiency before incorporation into the Carbopol® 940 gel base for the preparation of the polyherbal emulgel [11].

Table 5. Composition of Optimized Polyherbal Nanoemulsion (30 mL Batch)

Ingredient	F1 (0.5%)	F2 (1%)	F3 (3%)	F4 (5%)
Polyherbal extract	150 mg	300 mg	900 mg	1500 mg
Oil	7.86 mL	7.86 mL	7.86 mL	7.86 mL
Smix	12.33 mL	12.33 mL	12.33 mL	12.33 mL
Purified water	q.s. to 30 mL	q.s. to 30 mL	q.s. to 30 mL	q.s. to 30 mL

2.6. Evaluation of Nanoemulsion.

The optimized polyherbal nanoemulsion formulations were evaluated for particle size, polydispersity index (PDI), zeta potential, and entrapment efficiency. Particle size (Z-average) and PDI were determined by Dynamic Light Scattering (DLS) using a particle size analyzer after appropriate dilution with distilled water. The average particle size was used to assess droplet size, whereas the PDI indicated the uniformity of droplet size distribution and formulation homogeneity. Zeta potential was measured by Electrophoretic Light Scattering (ELS) using a Zetasizer at 25 ± 0.5°C to evaluate the surface charge and colloidal stability of the nanoemulsion. Entrapment efficiency was determined by the dialysis membrane method, in which 2 mL of the nanoemulsion was placed in a pre-soaked dialysis membrane and immersed in 50 mL of methanol under continuous stirring (300 rpm) for 6 h at 25 ± 2°C. The amount of unentrapped polyherbal extract diffused into the external medium was quantified using a UV–Visible spectrophotometer at the predetermined wavelength, and the entrapment efficiency was calculated using the following equation. [12], [13].

Entrapment Efficiency (%) = [(Total amount of extract − Free extract) / Total amount of extract] × 100

2.7. Development of Polyherbal Emulgel.

The optimized polyherbal nanoemulsion was incorporated into a Carbopol® 940 gel matrix to improve its viscosity, spreadability, and residence time on the skin, thereby making it suitable for topical application. Briefly, Carbopol® 940 (2% w/w) was gradually dispersed in the required quantity of distilled water under continuous stirring to obtain a lump-free dispersion and allowed to hydrate overnight at room temperature. Methyl paraben and propyl paraben, previously dissolved in propylene glycol, were then added to the hydrated gel base with continuous stirring. Triethanolamine was added dropwise to adjust the pH to 5.5–6.5, producing a clear, homogeneous gel. The optimized polyherbal nanoemulsion was slowly incorporated into the gel base with gentle stirring until a smooth and uniform emulgel was obtained. Four emulgel formulations containing 0.5%, 1%, 3%, and 5% (w/w) polyherbal extract were prepared while maintaining the optimized nanoemulsion composition constant. The prepared emulgels were filled into airtight containers and stored at room temperature for subsequent physicochemical and pharmacological evaluation [14].

2.8. Evaluation of Polyherbal Emulgel.

The prepared polyherbal emulgel formulations were evaluated for their physical appearance, pH, viscosity, spreadability, and extrudability. Physical appearance, including color, consistency, homogeneity, and the presence of any phase separation or grittiness, was assessed by visual inspection. The pH of the formulations was measured using a calibrated digital pH meter after dispersing 500 mg of emulgel in 10 mL of distilled water. Viscosity was determined using a Brookfield viscometer equipped with spindle No. 64 at 5 rpm and room temperature. Spreadability was evaluated using the parallel glass slide method by measuring the time required for the upper slide to move a fixed distance under a specified load. Extrudability was determined using collapsible aluminum tubes by measuring the amount of emulgel extruded under a constant applied weight. All measurements were performed in triplicate, and the results were expressed as mean ± standard deviation (SD) [15].

3. Results:

3.1. Preformulation Investigation.

Solubility Study

Table 6. Apparent solubility of the polyherbal extract in screened oils.

Oil	Solubility (mg/mL)
Sesame oil	>40.0
Olive oil	28
Castor oil	18
Coconut oil	12
Liquid paraffin	8

The apparent solubility of the polyherbal extract was determined by the shake-flask method. An excess amount of extract was added separately to each screened oil, agitated until equilibrium, centrifuged, and analyzed. The presentation reported the values shown in Table 6.

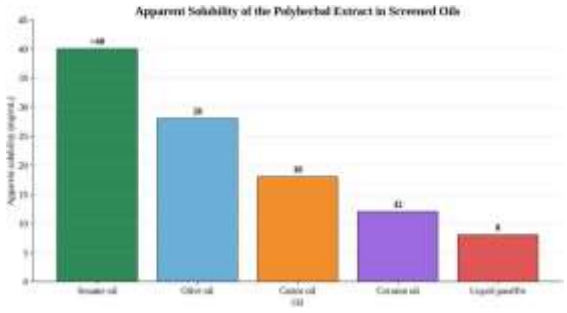

Figure 1. Apparent solubility of the polyherbal extract in screened oils.

Emulsification Efficiency

Surfactants and co-surfactants were screened by recording the volume of oil emulsified and percentage transmittance. Higher transmittance was interpreted as improved emulsification performance. The reported observations are presented in Table 7. The selection of an appropriate surfactant and co-surfactant is a crucial step in emulsion formulation, as these components significantly influence emulsification efficiency, droplet size, physical stability, and drug release characteristics. In the present study, Tween 80 exhibited superior emulsification efficiency compared with Tween 60, Span 20, and Kolliphor® EL. This enhanced performance may be attributed to its high hydrophilic-lipophilic balance (HLB ≈ 15), which favors the formation of stable oil-in-water emulsions. The higher transmittance observed with Tween 80 suggests the formation of finer emulsion droplets with improved homogeneity and optical clarity

Table 7. Emulsification efficiency of screened surfactants and co-surfactants.

Sr. No.	Surfactant/co-surfactant	Volume of oil emulsified (µL)	Transmittance (%T)
1	Tween 60	30	41.82
2	Tween 80	70	72.55
3	Span 20	40	47.68
4	Kolliphor® EL	20	39.86
5	Ethanol	30	31.46
6	Propylene glycol	50	51.46
7	PEG 400	20	38.54

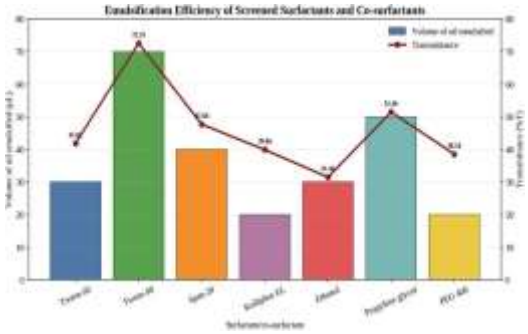

Figure 3. Emulsification efficiency of screened surfactants and co-surfactants.

3.3. Optimization of Polyherbal Extract

The 3 level Factorial design generated 13 experimental runs for the preparation Polyhebal extract loaded Nanoemulsion formulations. Based on study of previous literatures, three components were chosen as independent variables, and two responses were chosen as dependent variables. The developed formulations

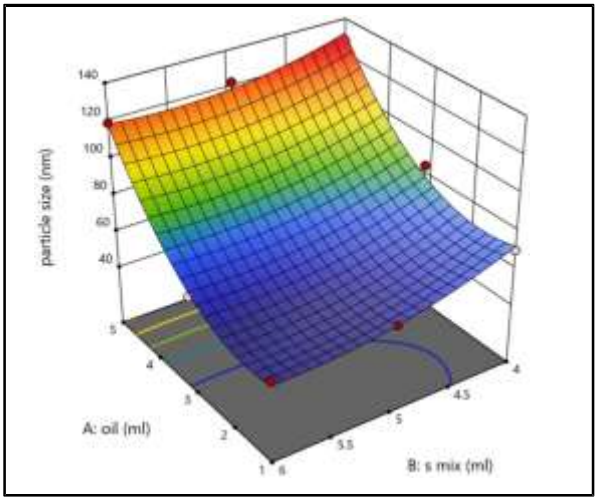

were characterized for vesicles size, zeta potential and entrapment efficiency. The best fit model was found to be the quadratic model for all three responses. The three-dimensional graphs produced by 3 level factorial desgn clearly show the effects of independent factors on vesicles size, zeta potential and entrapment efficiency. The plot representing the correlation between actual versus predicted value for the different responses and their residual plot is shown Table 8.

Table 8. Experimental design matrix and observed response values

Std	Run	Oil (mL)	Smix (mL)	Particle size (nm)Y1	Zeta potential (mV)Y2	Entrapment efficiency (%)Y3
3	1	5	4	128.1	-36.2	91.4
1	2	1	4	70.2	-20.1	68.12
4	3	1	5	54.1	-22.5	70.31
2	4	3	4	85.4	-28.0	87.3
11	5	3	5	62.7	-34.3	90.01
10	6	3	5	62.7	-34.3	90.01
8	7	3	6	58.3	-37.2	92.1
12	8	3	5	62.7	-34.3	90.01
9	9	5	6	119.2	-39.4	93.14
7	10	1	6	50.9	-26.6	72.01
6	11	5	5	122.5	-38.0	92.32
13	12	3	5	62.7	-34.3	90.01
5	13	3	5	62.7	-34.3	90.01

a) Response (Y_1): Effect of Independent Variables on Particle Size

Table 9. ANOVA for the quadratic model of particle size.

Source	Sum of squares	df	Mean square	F-value	p-value	Inference
Model	9071.31	5	1814.26	148.65	<0.0001	Significant
A: Oil	6311.53	1	6311.53	517.12	<0.0001	Significant
B: Smix	509.68	1	509.68	41.76	0.0003	Significant
AB	27.04	1	27.04	2.22	0.1802	Not significant
A^2	1463.24	1	1463.24	119.89	<0.0001	Significant
B^2	119.12	1	119.12	9.76	0.0167	Significant
Residual	85.44	7	12.21			
Lack of fit	85.44	3	28.48			
Pure error	0.0000	4	0.0000			
Corrected total	9156.75	12				

The supplied coded quadratic equation was:

Particle size = 63.44 + 32.43A - 9.22B + 2.60AB + 23.02A² + 6.57B²

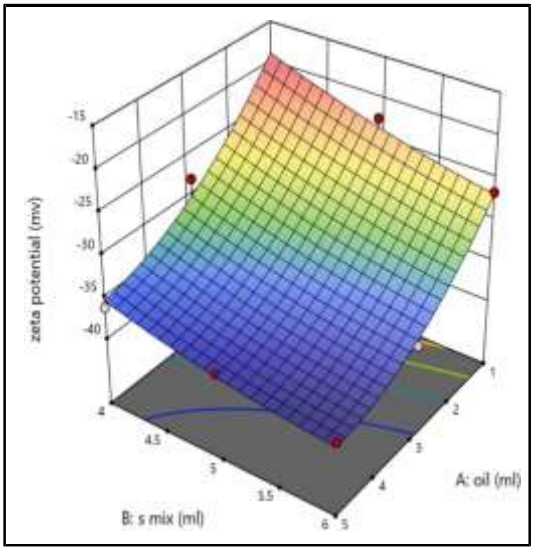

Figure 4. Three-dimensional response surface showing the effects of oil and Smix on particle size.

The particle-size model was significant (F = 148.65, p < 0.0001). Oil quantity was the dominant term and increased particle size, whereas increasing Smix reduced particle size within the studied range. The significant quadratic terms indicate curvature in the response. The interaction term was not significant (p = 0.1802). Dynamic light scattering is commonly used for submicrometric nanoemulsions droplets, but instrument settings, dispersant properties, temperature, and sample preparation should be reported for reproducibility [6,16]. Because the reported pure error was zero, a conventional lack-of-fit significance test could not be interpreted from the supplied table 9

b) Response (2): Impact of Independent Variables on Zeta Potential.

Table 10. ANOVA for the quadratic model of zeta potential.

Source	Sum of squares	df	Mean square	F-value	p-value	Inference
Model	428.46	5	85.69	63.12	<0.0001	Significant
A: Oil	328.56	1	328.56	242.02	<0.0001	Significant
B: Smix	59.53	1	59.53	43.85	0.0003	Significant
AB	2.72	1	2.72	2.01	0.1997	Not significant
A^2	26.07	1	26.07	19.20	0.0032	Significant
B^2	1.44	1	1.44	1.06	0.3371	Not significant
Residual	9.50	7	1.36			
Lack of fit	9.50	3	3.17			
Pure error	0.0000	4	0.0000			
Corrected total	437.97	12				

The supplied coded quadratic equation was:

Zeta potential = -34.02 - 7.40A - 3.15B + 0.8250AB + 3.07A² + 0.7224B²

Figure 5. Three-dimensional response surface showing the effects of oil and Smix on zeta potential.

c) Response (3): Impact of Independent Variables on Entrapment Efficiency.

Table 11. ANOVA for the quadratic model of Entrapment Efficiency

Source	Sum of Squares	df	Mean Square	F-value	p-value	Remark
Model	428.46	5	85.69	63.12	< 0.0001	significant
A-oil	328.56	1	328.56	242.02	< 0.0001	
B-s mix	59.53	1	59.53	43.85	0.0003	
AB	2.72	1	2.72	2.01	0.1997	
A^2	26.07	1	26.07	19.20	0.0032	
B^2	1.44	1	1.44	1.06	0.3371	
Residual	9.50	7	1.36			
Lack of Fit	9.50	3	3.17			
Pure Error	0.0000	4	0.0000			

Source	Sum of Squares	df	Mean Square	F-value	p-value	Remark
Cor Total	437.97	12				

Polynomial / Coded equation: EE = 89.99 + 11.07*A + 1.74*B -0.5375*AB - 8.62*A² - 0.2316*B²

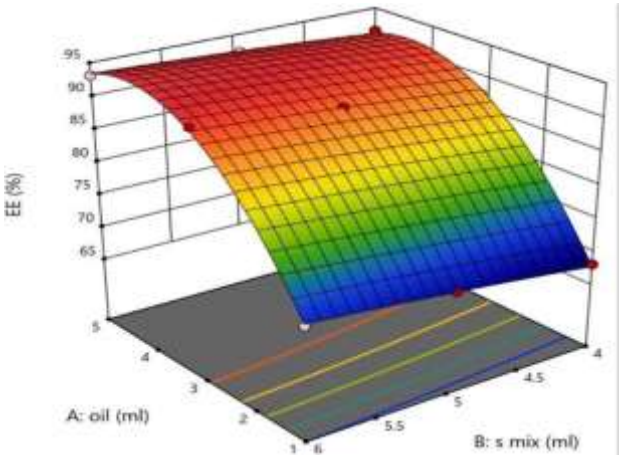

Figure 6. Three-dimensional response surface showing the effects of oil and Smix Entrapment Efficiency.

The positive linear oil coefficient indicates that entrapment efficiency increased with oil quantity over part of the design space, while the negative A^2 coefficient indicates an optimum rather than an indefinite increase. Smix produced a smaller positive linear effect. Statistical significance cannot be assigned to individual entrapment-efficiency terms because its ANOVA table was not supplied. The original presentation duplicated the zeta-potential ANOVA slide while displaying the entrapment-efficiency equation; the present paper retains the equation and clearly identifies the missing ANOVA data.

Optimized Solution Suggested by DoE

Table 12. Optimized Formulation Composition

Material	Optimized Quantity
Oil (A)	2.62 mL
Smix (B)	4.11 mL

Table 13. Predicted and Experimental Responses to the Optimized Formulation

Parameter	Optimized quantity	Predicted value	Actual value
Oil (mL)	2.62		
Smix (mL)	4.11		
Overall desirability	1.000		
Particle size (nm)		71.93	78.06
Zeta potential (mV)		-29.05	-32.24
Entrapment efficiency (%)		85.83	87.40

3.4. Optimized Polyherbal Nanoemulsion.

Table 14. Optimized Polyherbal Nanoemulsion.

Ingredient	F1 (0.5%)	F2 (1%)	F3 (3%)	F4 (5%)
Polyherbal extract	150 mg	300 mg	900 mg	1500 mg
Oil	7.86 mL	7.86 mL	7.86 mL	7.86 mL
Smix	12.33 mL	12.33 mL	12.33 mL	12.33 mL
Purified water	q.s. to 30 mL	q.s. to 30 mL	q.s. to 30 mL	q.s. to 30 mL

3.5. Evaluation Optimized Polyherbal Nanoemulsion.

Table 15. Evaluation Optimized Polyherbal Nanoemulsion.

Formulation	PS (nm)	PDI	ZP (mV)	EE(%)	Appearance
F1 (0.5%)	78.06	0.742	-30.8	79.8	Clear
F2 (1%)	79.8	0.481	-31.	83.2	Clear
F3 (3%)	78.1	0.615	-32.2	87.4	Clear
F4 (5%)	78.9	0.786	-33.1	90.3	Clear

3.6. Preparation of Polyherbal emulgel.

The optimized polyherbal extract-loaded nanoemulsion formulations (F1–F4) were incorporated into a gel base using Carbopol 940 (2% w/w) as the gelling agent to prepare the corresponding emulgel

formulations. Carbopol 940 was selected because of its excellent gelling properties, good viscosity, compatibility with topical formulations, and ability to provide sustained release of the encapsulated phytoconstituents. The prepared emulgels were subjected to further evaluation.

3.7. Characterization of Polyherbal emulgel formulation.

Table 16. Physicochemical characterization of polyherbal emulgel formulations

Evaluation Parameter	F1 (0.5%)	F2 (1%)	F3 (3%)	F4 (5%)
Physical appearance	Creamish	Creamish	Creamish	Creamish
Homogeneity	Good	Good	Good	Good
pH	6.22 ± 0.04	6.25 ± 0.05	6.20 ± 0.06	6.15 ± 0.05
Viscosity (cP)	36,700	37,800	34,100	33,200
Shear rate (rpm)	5	5	5	5
Spreadability (g·cm/s)	5.8	5.4	5.1	4.7

The prepared polyherbal nanoemulgel formulations (F1–F4) were visually evaluated for physical appearance and homogeneity. The results are presented in Table 16. All formulations exhibited a creamish appearance with a smooth and uniform texture. No visible lumps, grittiness, phase separation, creaming, or precipitation
were observed, indicating successful incorporation of the optimized polyherbal nanoemulsion into the Carbopol 940 gel base.The homogeneity of all formulations was found to be good, demonstrating uniform distribution of the nanoemulsion throughout the gel matrix. The formulations were free from coarse particles and showed consistent texture upon visual examination. These findings indicate that the selected concentration of Carbopol 940 (2% w/w) produced stable and homogeneous nanoemulgels suitable for topical application.

3.8. Extended analytical evaluation of the supplied formulation dataset.

A secondary quantitative analysis was performed using only the numerical values already reported in the experimental design matrix and the preliminary emulgel-characterization table. No new laboratory observations were generated. The calculations were used to describe response variability, reconstruct the missing entrapment-efficiency ANOVA, compare model adequacy, examine prediction error, and assess concentration-dependent trends in pH, viscosity, and spreadability. Because the five center-point runs contained identical rounded values, the results should be interpreted as an analytical extension of the supplied dataset rather than as independent experimental validation.

3.8.1. Descriptive distribution of factorial-design responses

Table 17. Descriptive statistics calculated from the 13-run experimental design matrix.

Response	n	Mean	SD	Minimum	Maximum	Range	CV (%)
Particle size (nm)	13	77.09	27.62	50.90	128.10	77.20	35.83
Zeta potential (mV)	13	-32.27	6.04	-39.40	-20.10	19.30	18.72*
Entrapment efficiency (%)	13	85.90	9.13	68.12	93.14	25.02	10.63

The particle-size response showed the greatest relative dispersion, with a range of 77.20 nm and a coefficient of variation of 35.83%. This wide distribution was consistent with the strong positive oil coefficient in the quadratic model and indicates that droplet size was highly sensitive to formulation composition. Entrapment efficiency showed the lowest relative dispersion (CV 10.63%), although its minimum value of 68.12% occurred at the low-oil condition. The zeta-potential values remained negative throughout the design space, ranging from -20.10 to -39.40 mV. The descriptive means are weighed by the repeated center points and therefore should not replace the factorial model when judging factor effects.

3.8.2 Factor-level response patterns

Table 18. Mean responses obtained at the three oil levels.

Oil (mL)	Runs (n)	Mean particle size (nm)	Mean zeta potential (mV)	Mean entrapment efficiency (%)
1	3	58.40	-23.07	70.15
3	7	65.31	-33.81	89.92
5	3	123.27	-37.87	92.29

Increasing the oil level from 1 to 5 mL increased the pooled mean particle size by 64.87 nm, shifted the mean zeta potential by 14.80 mV toward a more negative value, and increased mean entrapment efficiency by 22.14 percentage points. The change from 3 to 5 mL oil was especially important for particle size, where the mean rose from 65.31 to 123.27 nm. These pooled means support the model conclusion that oil was the dominant formulation factor, while also demonstrating the practical trade-off between greater incorporation of extract and enlargement of dispersed droplets

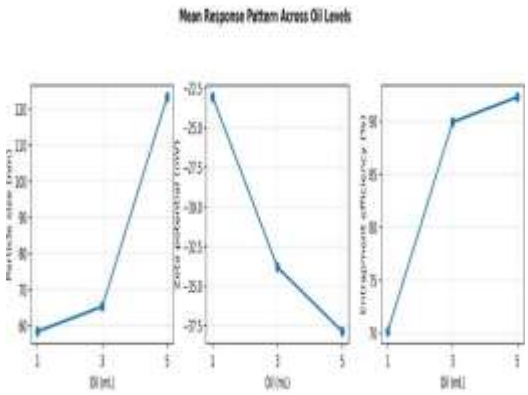

Figure 7. Pooled mean particle size, zeta potential, and entrapment efficiency across oil levels.

3.8.4. Comparative adequacy of the three response models

Table 19. Model-fit statistics calculated from the reported design matrix.

Response	R^2	Adjusted R^2	RMSE	Model CV (%)	Overall F	Model p-value
Particle size	0.9907	0.9840	3.49 nm	4.53	148.65	<0.0001
Zeta potential	0.9783	0.9628	1.17 mV	3.61	63.12	<0.0001
Entrapment efficiency	0.9987	0.9977	0.44 %	0.51	1040.93	<0.0001

All three quadratic models explained more than 97% of the observed response variation. Entrapment efficiency displayed the highest coefficient of determination and the lowest model CV, followed by particle size and zeta potential. The RMSE values were small relative to the observed response ranges, supporting good numerical agreement between fitted and reported values. Nevertheless, the apparent precision is partly influenced by the five identical center-point observations. Independent replicate batches with unrounded instrument readings are required to estimate experimental variability and establish a meaningful lack-of-fit test.

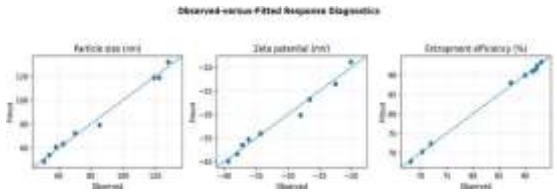

Figure 8. Observed-versus-fitted diagnostics for the quadratic response models.

The observed-versus-fitted plots showed close alignment with the line of identity for all three responses. The particle-size plot displayed the largest visible scatter, which was consistent with its higher RMSE and wider response range. Several center-point symbols overlap because the same values were reported five times. The plots therefore demonstrate mathematical fit to the supplied dataset but should not be interpreted as evidence of between-batch reproducibility.

3.8.5. Analytical assessment of optimization verification

Table 20. Prediction-error analysis for the optimized formulation.

Response	Predicted	Actual	Actual - predicted	Absolute difference	Relative deviation (%)	Actual/predicted
Particle size (nm)	71.93	78.06	+6.13	6.13	8.52	1.085
Zeta potential (mV)	-29.05	-32.24	-3.19	3.19	10.98*	1.110*
Entrapment efficiency (%)	85.83	87.40	+1.57	1.57	1.83	1.018

**Relative deviation and ratio for zeta potential were calculated using absolute magnitudes.*

Entrapment efficiency showed the closest prediction, with an absolute difference of 1.57 percentage points and a relative deviation of 1.83%. Particle size was 6.13 nm above the predicted value, while the magnitude of zeta potential was 3.19 mV greater than predicted. The direction of all three deviations remained favorable for entrapment and electrostatic magnitude but less favorable for particle-size minimization. Because a predefined model-verification acceptance limit was not reported, the deviations should be presented transparently rather than classified as passing or failing. Confirmation with at least three independently prepared validation batches would allow calculation of mean prediction error and confidence intervals.

3.8.6. Concentration-dependent trends in emulgel properties

The four emulgel formulations were further examined as an exploratory concentration series. Simple linear regression was applied to the stated formulation concentrations (0.5%, 1%, 3%, and 5%) and the reported pH, viscosity, and spreadability values. With only four observations and no replicate variability for viscosity or spreadability, the regression statistics are descriptive and should not be treated as confirmatory.

Table 21. Exploratory linear-trend statistics for the emulgel characterization data.

Property	Slope per 1% concentration	Correlation (r)	R^2	p-value	Data-based interpretation
pH	-0.0305	-0.973	0.947	0.027	Progressive mild decrease
Viscosity (cP)	-971.43	-0.926	0.857	0.074	Overall decrease; F2 local maximum
Spreadability (g·cm/s)	-0.2187	-0.966	0.934	0.034	Progressive decrease

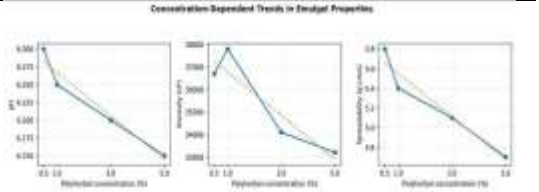

Figure 9. Exploratory concentration trends for pH, viscosity, and spreadability.

The pH decreased by an estimated 0.0305 units for each 1% increase in formulation concentration, while spreadability decreased by approximately 0.219 g.cm/s per 1% increase. Viscosity showed an overall negative slope of about 971 cP per 1% increase, but F2 was more viscous than F1, confirming that the pattern was not strictly monotonic. The small p-values for pH and spreadability reflect the orderly four-point trend, but the sample size is too limited for robust inference. These findings indicate that increasing the extract-loaded phase can influence neutralization balance, gel microstructure, and ease of spreading.

Table 22. Correlation analysis among the preliminary emulgel properties.

Variable pair	Pearson r	Direction	Interpretation within F1-F4
Concentration vs pH	-0.973	Strong negative	Higher concentration accompanied lower pH

Variable pair	Pearson r	Direction	Interpretation within F1-F4
Concentration vs viscosity	-0.926	Strong negative	Overall viscosity declined despite the F2 peak
Concentration vs spreadability	-0.966	Strong negative	Higher concentration reduced spreading rate
Viscosity vs spreadability	+0.823	Positive	More viscous samples also showed greater spreadability in this limited series
pH vs spreadability	+0.999	Strong positive	Both properties decreased together across the four formulations

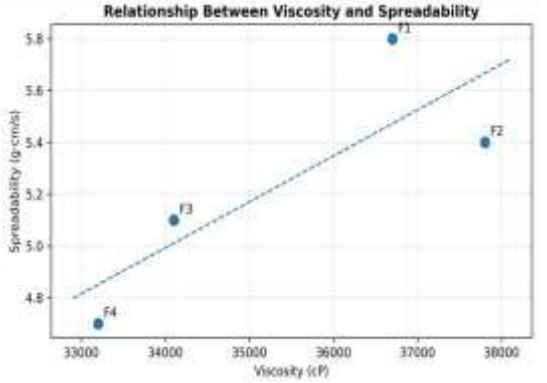

Figure 10. Relationship between viscosity and spreadability in formulations F1-F4.

The positive viscosity-spreadability correlation differs from the inverse relationship often expected for otherwise comparable semisolid systems. In this dataset, both variables generally decreased as formulation concentration increased, and the F2 viscosity maximum did not produce a corresponding increase in spreadability above F1. The apparent correlation may therefore reflect simultaneous changes in composition rather than a direct causal relationship. A complete rheological profile should include viscosity at several shear rates, flow-curve modeling, thixotropic recovery, yield stress, and replicate spreadability testing

3.8.7 Cross-validated predictive assessment

Leave-one-out prediction diagnostics were calculated from the same quadratic models to provide a more conservative indication of predictive performance. For each run, the fitted value was estimated after accounting for the leverage of that observation, and the resulting prediction residuals were combined as the prediction error sum of squares (PRESS). Predicted R^2 was then calculated as 1 - PRESS/corrected total sum of squares. These values are still affected by the repeated identical center points, but they offer a stricter check than ordinary R^2 alone.

Table 23. Cross-validated prediction diagnostics for the three responses.

Response	PRESS	Predicted R^2	Mean absolute residual	Maximum absolute residual	Interpretation
Particle size	803.44	0.9123	1.90 nm	6.18 nm	Good predictive agreement
Zeta potential	87.24	0.8008	0.66 mV	2.15 mV	Acceptable but comparatively weaker
Entrapment efficiency	13.63	0.9864	0.22 %	0.72%	Very strong predictive agreement

The predicted R^2 values followed the same order as the model-fit statistics, with entrapment efficiency showing the strongest predictive performance and zeta potential the weakest. The difference between adjusted R^2 and predicted R^2 was approximately 0.072 for particle size, 0.162 for zeta potential, and 0.011 for entrapment efficiency. The larger reduction for zeta potential indicates greater sensitivity to individual design points and supports the need for independent verification. Even so, all predicted R^2 values remained positive and the mean absolute residuals were small relative to the observed ranges.

3.7.8 Model-based response trade-off analysis

The fitted equations were used to calculate response regions across the studied factor space. This analysis does not add experimental observations; it visualizes the simultaneous consequences of changing oil and Smix. The optimized point was located in a compromise region rather than at the individual maximum or minimum of every response. Low oil and high Smix favored small particle size, whereas higher oil favored entrapment efficiency and a more negative zeta potential.

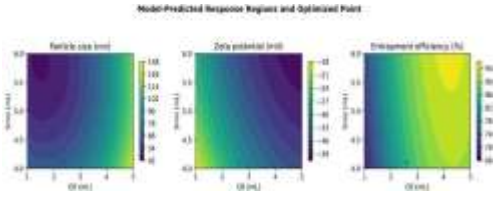

Figure 11. Model-predicted response regions for particle size, zeta potential, and entrapment efficiency; the marker indicates the optimized point.

Table 24. Model-predicted responses at selected factor combinations.

Factor combination	Oil (mL)	Smix (mL)	Particle size (nm)	Zeta potential (mV)	Entrapment efficiency (%)
Low oil-low Smix	1.00	4.00	72.41	-18.85	67.79
Low oil-high Smix	1.00	6.00	48.77	-26.80	72.35
Design center	3.00	5.00	63.44	-34.02	89.99
Numerical optimum	2.62	4.11	71.95	-28.99	85.75
High oil-low Smix	5.00	4.00	132.07	-35.30	91.01
High oil-high Smix	5.00	6.00	118.84	-39.95	93.41

At the low-oil/high-Smix corner, the model predicted the smallest particle size but comparatively low entrapment efficiency. At the high-oil/high-Smix corner, entrapment and zeta-potential magnitude were greatest, but the predicted particle size exceeded 100 nm. The selected optimum therefore avoided the high particle-size penalty associated with 5 mL oil while retaining an entrapment efficiency above 85%. This trade-off explains why the desirability solution did not coincide with the maximum oil and Smix levels.

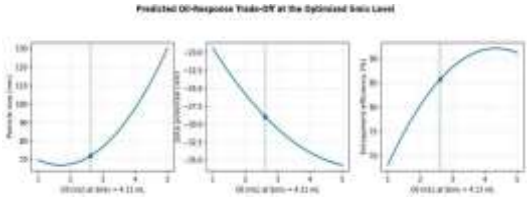

Figure 12. Predicted response changes with oil at the optimized Smax level of 4.11 mL.

At Smix 4.11 mL, increasing oil initially improves entrapment efficiency and makes the zeta potential more negative, but particle size rises sharply as oil approaches the upper design level. The oil value of 2.62 mL lies before the steepest particle-size increase and near the region where entrapment efficiency has already improved substantially. This model-based profile supports the numerical optimum as a balanced formulation choice, subject to confirmation by replicated manufacture and analytical testing.

4. Discussion

The present study successfully developed and optimized a polyherbal emulgel containing methanolic stem bark extracts of *Limonia acidissima*, *Moringa oleifera*, and *Pithecellobium dulce* using a Quality-by-Design (QbD) approach. Systematic preformulation studies, statistical optimization, and incorporation of the optimized nanoemulsion into a Carbopol® 940 gel base resulted in a formulation with desirable physicochemical properties for topical drug delivery. The preformulation study (Table 6) identified sesame oil as the most suitable oil phase because it exhibited the highest apparent solubility (>40 mg/mL) for the polyherbal extract. High drug solubility in the oil phase enhances drug loading, minimizes precipitation during storage, and improves formulation stability. Sesame oil has been reported as an excellent carrier oil due to its high content of unsaturated fatty acids and antioxidant constituents, which improve the solubilization of lipophilic phytochemicals and enhance dermal permeation [16]. Selection of suitable surfactants and co-surfactants is essential for obtaining stable nanoemulsions. As shown in Table 7, Tween 80 exhibited the highest emulsification efficiency (72.55% transmittance), while propylene glycol was selected as the most suitable co-surfactant. Tween 80 possesses a high hydrophilic-lipophilic balance (HLB), enabling efficient reduction of interfacial tension and formation of stable oil-in-water nanoemulsions with fine droplet distribution. Propylene glycol further improves interfacial flexibility and enhances solubilization of the herbal constituents, thereby contributing to formulation stability [17]. The optimization study (Tables 8–13) demonstrated that both oil concentration and Smix significantly influenced particle size, zeta potential, and entrapment efficiency. Statistical analysis confirmed that the quadratic model adequately described the responses with highly significant model p-values ($p < 0.0001$). Increasing oil concentration resulted in larger particle size, whereas increasing Smix reduced particle size by providing sufficient surfactant molecules to stabilize newly formed droplets. Similar effects of formulation variables on nanoemulsion characteristics have been widely reported in Design of Experiments (DoE)-based optimization studies [18].The optimized formulation containing 2.62 mL oil and 4.11 mL Smix (Tables 12 and 13) achieved an overall desirability value of 1.000. Experimental validation showed close agreement between predicted and observed responses, producing a particle size of 78.06 nm, zeta potential of −32.24 mV, and entrapment efficiency of 87.40%. These findings confirm the predictive accuracy of the optimization model and demonstrate the effectiveness of the QbD approach in developing reproducible nanoemulsion formulations [19].Evaluation of the optimized nanoemulsions (Table 15) showed particle sizes below 80 nm, indicating successful preparation of nanosized droplets suitable for topical drug delivery. Such small droplets provide a larger surface area, improve skin adhesion, facilitate penetration through the stratum corneum, and enhance local bioavailability of phytoconstituents [20]. The zeta potential values ranged from −30.8 to −33.1 mV, indicating sufficient electrostatic repulsion to prevent droplet aggregation and maintain colloidal stability during storage [21]. Entrapment efficiency progressively increased from

79.8% to 90.3% with increasing extract concentration, indicating efficient encapsulation of the phytoconstituents within the oil phase and suggesting improved potential for sustained topical drug release [22].Following optimization, the nanoemulsion was successfully incorporated into a Carbopol® 940 gel matrix to prepare the polyherbal emulgel. As presented in Table 16, all formulations exhibited a creamish appearance, excellent homogeneity, and no evidence of phase separation or grittiness, demonstrating good compatibility between the nanoemulsion and gel base. Carbopol® 940 is widely employed in topical formulations because it provides excellent viscosity, physical stability, and uniform distribution of dispersed droplets [23].The prepared emulgels exhibited skin-compatible pH values ranging from 6.15 to 6.25, minimizing the risk of skin irritation during topical application. Furthermore, viscosity values between 33,200 and 37,800 cP and spreadability values ranging from 4.7 to 5.8 g·cm/s indicated appropriate rheological properties for easy application and prolonged residence at the application site. Although spreadability decreased slightly with increasing extract concentration, all formulations remained suitable for topical administration [24].Overall, the additional statistical analyses (Tables 17–24) confirmed the robustness of the optimization process, with high model accuracy and excellent predictive performance. The developed polyherbal emulgel possessed nanosized droplets, high entrapment efficiency, adequate colloidal stability, skin-compatible pH, and desirable rheological characteristics, indicating its potential as an effective topical drug delivery system for future wound-healing and antimicrobial applications [25].

5. Conclusion

The present study successfully developed and optimized a polyherbal emulgel containing methanolic stem bark extracts of *Limonia acidissima*, *Moringa oleifera*, and *Pithecellobium dulce* using a Quality-by-Design (QbD) approach. The optimized formulation exhibited nanosized droplets, high entrapment efficiency, satisfactory zeta potential, skin-compatible pH, and suitable rheological properties, indicating excellent physicochemical stability and topical applicability. Incorporation of the optimized nanoemulsion into a Carbopol® 940 gel base produced a homogeneous and stable emulgel with desirable spreadability and viscosity. Overall, the findings suggest that the developed polyherbal emulgel is a promising topical drug delivery system and provides a suitable platform for further in vivo wound-healing, antimicrobial, and clinical investigations.

6. Acknowledgments

We are grateful to Oriental University, Indore, for providing laboratory facilities and to the Botanical Survey of India, Western Regional Centre, Pune, for authenticating the plant specimens

References

1. Gonzalez ACDO, Costa TF, Andrade ZA, Medrado ARAP. Wound healing - A literature review. Anais Brasileiros de Dermatologia. 2016;91(5):614-620. doi:10.1590/abd1806-4841.20164741.
2. Huynh P, Phie J, Krishna SM, et al. Systematic review and meta-analysis of mouse models of diabetes-associated ulcers. BMJ Open Diabetes Research and Care. 2020;8(1):e000982. doi:10.1136/bmjdrc-2019-000982.
3. Jain AK, Dixit A, Mehta SC. Wound healing activity of aqueous extracts of leaves and roots of Coleus aromaticus in rats. Acta Poloniae Pharmaceutica - Drug Research. 2012;69(6):1119-1123.
4. James O, Victoria IA. Excision and incision wound healing potential of Saba florida (Benth.) leaf extract in Rattus norvegicus. International Journal on Pharmaceutical and Biomedical Research. 2010;1(4):101-107.
5. Ajazuddin, Alexander A, Khichariya A, Gupta S, Patel RJ, Giri TK, Tripathi DK. Recent expansions in an emergent novel drug delivery technology: Emulgel. J Control Release. 2013;171(2):122-132. doi:10.1016/j.jconrel.2013.06.030.
6. Tadros T, Izquierdo P, Esquena J, Solans C. Formation and stability of nano-nanoemulsionss. Adv Colloid Interface Sci. 2004;108-109:303-318. doi:10.1016/j.cis.2003.10.023.
7. McClements DJ. Nanoemulsionss versus micronanoemulsionss: terminology, differences, and similarities. Soft Matter. 2012;8(6):1719-1729. doi:10.1039/C2SM06903B.
8. Honary S, Zahir F. Effect of zeta potential on the properties of nano-drug delivery systems - a review (Part 1). Trop J Pharm Res. 2013;12(2):255-264. doi:10.4314/tjpr.v12i2.19.
9. International Council for Harmonisation of Technical Requirements for Pharmaceuticals for Human Use. ICH Q8(R2): Pharmaceutical Development. Geneva: ICH; 2009.
10. Myers RH, Montgomery DC, Anderson-Cook CM. Response Surface Methodology: Process and Product Optimization Using Designed Experiments. 4th ed. Hoboken (NJ): John Wiley & Sons; 2016.
11. Lambers H, Piessens S, Bloem A, Pronk H, Finkel P. Natural skin surface pH is on average below 5, which is beneficial for its resident flora. Int J Cosmet Sci. 2006;28(5):359-370. doi:10.1111/j.1467-2494.2006.00344.x.
12. Rathi BS, Bodhankar SL, Baheti AM. Evaluation of aqueous leaves extract of Moringa oleifera Linn for wound healing in albino rats. Indian J Exp Biol. 2006;44(11):898-901.
13. International Council for Harmonisation of Technical Requirements for Pharmaceuticals for

Human Use. ICH Q1A(R2): Stability Testing of New Drug Substances and Products. Geneva: ICH; 2003.

14. Organisation for Economic Co-operation and Development. Test No. 404: Acute Dermal Irritation/Corrosion. OECD Guidelines for the Testing of Chemicals, Section 4. Paris: OECD Publishing; 2002. doi:10.1787/9789264070622-en.
15. Clinical and Laboratory Standards Institute. Methods for Dilution Antimicrobial Susceptibility Tests for Bacteria That Grow Aerobically. 12th ed. CLSI standard M07. Wayne (PA): CLSI; 2024.
16. International Organization for Standardization. ISO 22412:2025. Particle size analysis - Dynamic light scattering (DLS). Geneva: ISO; 2025.
17. Franz TJ. Percutaneous absorption: on the relevance of in vitro data. J Invest Dermatol. 1975;64(3):190-195. doi:10.1111/1523-1747.ep12533356.
18. McClements DJ. Nanoemulsions versus microemulsions: Terminology, differences, and similarities. Soft Matter. 2012;8(6):1719–1729.
19. Solans C, Solé I. Nano-emulsions: Formation by low-energy methods. Current Opinion in Colloid & Interface Science. 2012;17(5):246–254.
20. Singh Y, Meher JG, Raval K, Khan FA, Chaurasia M, Jain NK, Chourasia MK. Nanoemulsion: Concepts, development and applications in drug delivery. Journal of Controlled Release. 2017;252:28–49.
21. Gupta A, Eral HB, Hatton TA, Doyle PS. Nanoemulsions: Formation, properties and applications. Soft Matter. 2016;12(11):2826–2841.
22. Tadros T, Izquierdo P, Esquena J, Solans C. Formation and stability of nano-emulsions. Advances in Colloid and Interface Science. 2004;108–109:303–318.
23. Jaiswal M, Dudhe R, Sharma PK. Nanoemulsion: An advanced mode of drug delivery system. 3 Biotech. 2015;5:123–127.
24. Honary S, Zahir F. Effect of zeta potential on the properties of nano-drug delivery systems. Tropical Journal of Pharmaceutical Research. 2013;12(2):255–264.
25. Shakeel F, Ramadan W, Ahmed MA. Investigation of true nanoemulsions for transdermal drug delivery. Expert Opinion on Drug Delivery. 2015;12(7):1103–1112.